FLAME ACCELERATION, DETONATION LIMIT AND HEAT LOSS FOR HYDROGEN-OXYGEN MIXTURE AT CRYOGENIC TEMPERATURE OF 77 K

Xiaobo Shen[a,b,c], Wenju Fu[b], Haifeng Liu[d], Jennifer X. Wen[a,1]

[a]*Centre for Energy Resilience, School of Mechanical Engineering Sciences, University of Surrey, Guildford, UK*
[b]*School of Resources & Environmental Engineering, East China University of Science and Technology, Shanghai, 200237, PR China*
[c]*Shanghai Institute of Pollution Control and Ecological Security, Shanghai 200092, PR China*
[d]*Shanghai Engineering Research Center of Coal Gasification, East China University of Science and Technology, Shanghai 200237, PR China*

ABSTRACT

Experiments are performed in hydrogen-oxygen mixtures at the cryogenic temperature of 77 K with the equivalence ratio of 1.5 and 2.0. The optical fibers, pressure sensors and the smoked foils are used to record the flame velocity, overpressure evolution curve and detonation cells, respectively. The 1st and 2nd shock waves are captured and they finally merge to form a stronger precursor shock wave prior to the onset of detonation. The cryogenic temperature will cause the larger expansion ratio which results in the occurrence of strong flame acceleration. The stuttering mode, the galloping mode and the deflagration mode are observed when the initial pressure decreases from 0.50 atm to 0.20 atm with the equivalence ratio of 1.5, and the detonation limit is within 0.25-0.30 atm. The heat loss effect on the detonation limit is analysed. In addition, the regularity of detonation cell is investigated, and the larger post-shock specific heat ratio γ_{VN} and the lower normalized activation energy ε_i at lower initial pressure will cause the more regular detonation cell. Also, the detonation cell width is predicted by a model of $\lambda = A(\chi_2) \cdot \Delta_i$, and the prediction results are mainly consistent with the experimental results.

1.0 INTRODUCTION

Compared the gaseous hydrogen, the liquid hydrogen has obvious advantages in hydrogen transportation and storage, as a result of the features of higher density and smaller volume. In recent years, the liquid hydrogen has been applied in fields such as agriculture, healthcare, food, electronics and aerospace. However, with the gradual popularization of liquid nitrogen in all aspects of daily life, there are many safety risks in the hydrogen storage, transportation and utilization. The incident release of liquid hydrogen will result in the formation of hydrogen-air flammable mixture with the cryogenic temperature, which could further lead to the fire or explosion after ignited by the electrostatic spark, fire or high temperature.

So far, however, limited studies have been performed on flame acceleration (FA) and the deflagration to detonation transition (DDT) of hydrogen mixture at cryogenic temperature. Kuznetsov et al. [1] had been investigated the hydrogen-air detonation at cryogenic temperature and found the larger expansion ratio (σ) could shorten the run-up distance to detonation at cryogenic temperature compared with room temperature. Subsequently, our previous study [2] also investigated the strong flame acceleration and detonation limit of hydrogen-oxygen mixture at cryogenic temperature and different initial pressures (P_0). The 1st and 2nd shock waves had been captured and the strong FA caused by larger expansion ratio at cryogenic temperature leads to the formation of supersonic flame and detonation. The galloping mode and fast flame mode had been observed at 0.6-1.0 atm and 0.4 atm, respectively. However, the experimental data at cryogenic temperature are still limited.

[1] Correspondence j.wen@surrey.ac.uk

The appearance of detonation limit will lead to some specific phenomenon such as the detonation velocity deficit in stable mixture and the unstable detonation modes in unstable mixture. Manson and Guénoche [3] found that the larger heat and moment losses caused by the boundary layer is responsible for the detonation failure in stable mixture, while, in unstable mixture, the appearance of detonation limit is caused by the elimination of transverse waves. Kogarko and Zeldovich [4] firstly proposed that the onset of the single head spin mode can be considered as the minimum criterion for the formation of detonation. They found that when the single head spin mode appears, there is a relationship of $d_{min} = \lambda/\pi$ between the minimum tube diameter (d_{min}) and the detonation cell size (λ). In the relatively large tube ($\lambda \ll d$), the limit of the minimum tube diameter will not exist and the critical condition for the formation of detonation is mainly associated with the occurrence of strong FA regime and the enough run-up distance to supersonic state [5, 6]. At cryogenic temperature condition, as a result of larger temperature difference between the cold wall and the hot flame, the heat loss effect will be enhanced. However, the heat loss effect on the detonation limit at cryogenic temperature has not yet been elucidated.

For the aim of investigating and exploring the strong FA and detonation limit at cryogenic temperature condition, the flame speed and overpressure in hydrogen-oxygen mixture with the equivalence ratio of 1.5, and 2.0 are analysed in present study. And, the 1st and 2nd shock waves, the unstable detonation mode, the heat loss effect on detonation limit and the detonation cell regularity are analysed.

2.0 EXPERIMENTAL METHODS

The schematic diagram of the experimental apparatus is showed in Fig. 1. And, Fig. 2 shows the layout of the optical fibers (OF) and PCB pressure sensors (PS). The time-of-arrival of flame propagating at different positions is recorded by the optical fibers and the overpressure evolution traces are captured by two PCB pressure sensors. In order to analyse the regularity of detonation cells, the detonation cells are recorded with the smoked foils placed at the end of tube. The hydrogen and oxygen will be premixed in a premixed gas cylinder with the partial pressure method. The closed tube filled with the premixed gas will be immersed in the liquid nitrogen for around 6 minutes before ignition. Since the cryogenic temperature of 77 K is less than the critical temperature of oxygen, it should be noted that the problem of oxygen liquefaction at a certain equivalence ratio and initial pressure when designing the experimental cases. In present study, the experiments were performed at different initial pressures and around 77 K with the equivalence ratio of 1.5, and 2.0. For more detailed information about experimental set up and measurements techniques, readers should refer to our recent publication [2].

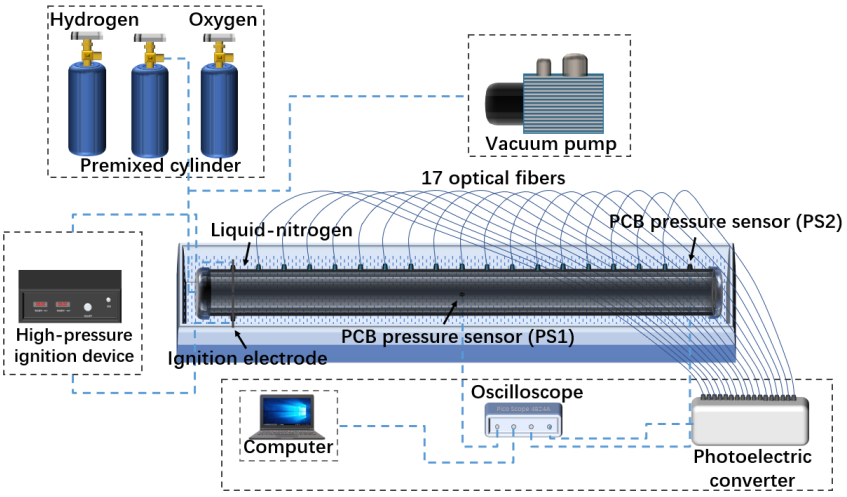

Figure 1. Schematic diagram of the experimental apparatus.

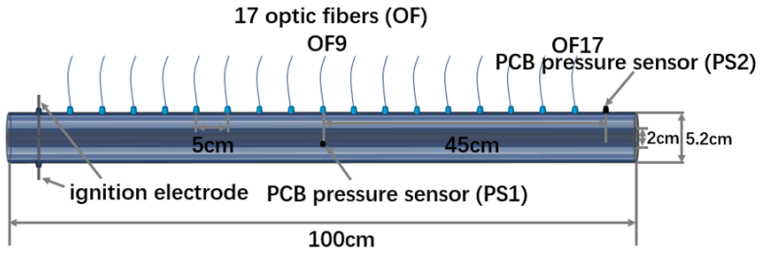

Figure 2. Schematic diagram of the optical fibers (OF) and the PCB pressure sensors (PS) distribution.

3.0 RESULTS AND DISCUSSION

3.1 Shock wave and flame

Kellenberger and Ciccarelli [7] found that there are two discrete shock waves propagating ahead the flame and these two shock waves finally merge with each other to propagate forward. Subsequently, Cheng et al. [8, 9] also observed the two discrete shock waves and they defined them as the 1st and 2nd shock waves, respectively. The experimental results showed that when propagating forward to a certain distance, the 1st and 2nd shock waves will form a stronger precursor shock wave. They illustrated that the formation of the 1st shock wave is mainly associated with a set of weak compression waves during flame expansion stage, while the disturbance of flame tip at flame acceleration stage results in the formation of the 2nd shock wave.

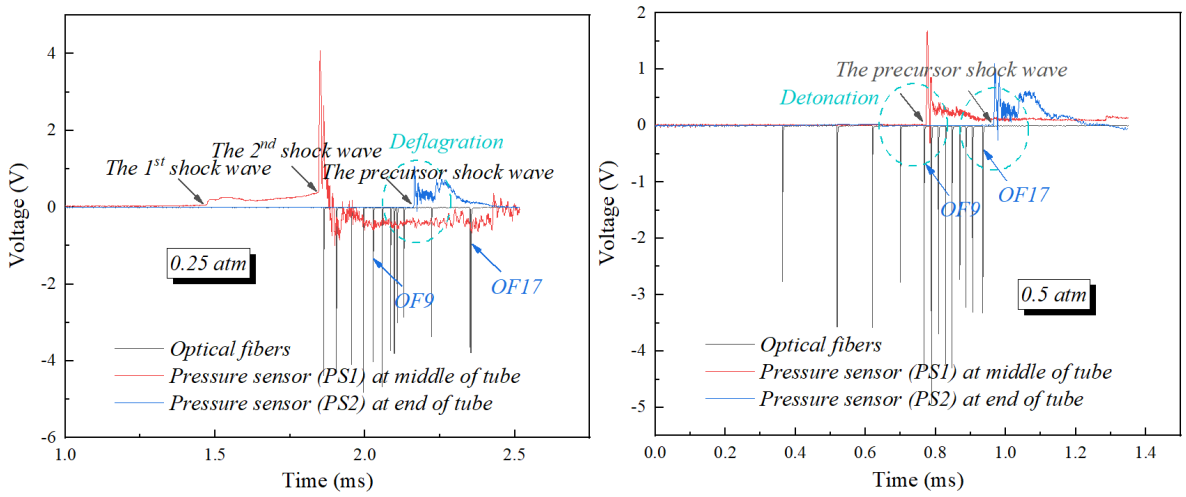

(a) (b)

Figure 3. The signals of the overpressure and optical fibers at different P_0 and 77 K with the equivalence ratio of 1.5.

In present study, the 1st and 2nd shock waves also were captured at cryogenic temperature condition. Fig. 3 shows the signals of the overpressure and optical fibers at 77 K and different P_0 with the equivalence ratio of 1.5. In Fig. 3(a), there is a small "step" appearing in the overpressure evolution curve measured by the pressure sensor (PS1) installed at the middle position of tube. The formation of the "step" is associated with the time delay between the 1st shock wave and the 2nd shock wave arriving at the middle position of tube. And, in the curve of overpressure evolution measured by the pressure sensor (PS2) installed at the end position of tube, the "step" disappears which illustrates that these two discrete shock waves have merged with each other to form a stronger precursor shock wave. Similarly, in Fig. 3(b), the overpressure evolution curve measured by PS1 illustrates that the 2nd shock wave has caught up with the 1st shock wave to form a stronger precursor shock wave before propagating at the middle position of tube. In Fig. 3(b), the time-of-arrival of flame propagating at different positions is recorded by the optical fibers. From Fig. 2, the 9th optical fiber (OF9) is installed at the same position with PS1 and the 17th optical fiber (OF17) is installed at the location which is 5

cm away from PS2. It can be found from Fig. 3(b) that at the same time, the flame and the precursor shock wave all propagate at the middle position of tube which means the flame are coupled with the precursor shock wave at this position and the detonation has formed. At Fig. 3(b), the precursor shock wave arrives at the position of PS2 after the flame propagates at the position of OF17 and this phenomenon is not consistent with that at Fig. 3(a). These two different phenomenon indicate the coupled and decoupled states between the flame and the precursor shock wave, which show the detonation and deflagration modes, respectively.

Fig. 4 shows the positions of shock waves and flame at corresponding time instants with different P_0 and 77 K with the equivalence ratio of 1.5. From Fig. 4(a), at 0.25 atm, the 1st shock wave is decoupled with the 2nd shock wave at the position of PS1, and with flame propagates forward, the 2nd shock wave finally catches up with the 1st shock wave at the position of PS2 to form a stronger precursor shock wave. However, at this moment, there is some distance between the flame and the formed precursor shock wave which indicates the detonation has not formed. From Fig. 4(b), at 0.3 atm, the flame and the precursor shock wave have been in coupled state at the position of PS2 finally which indicates the detonation forms. Based on the comparison between Fig. 4(a) and Fig. 4(b), the 1st and 2nd shock waves propagating ahead of flame firstly need to merge to form a stronger precursor shock wave before the detonation forms, and after the precursor shock wave forms, the flame then needs to catch up with the formed precursor shock wave to form the detonation. When the precursor shock wave is coupled with the flame, this means the detonation forms. With the further increase in the initial pressure to 0.5 atm, from Fig. 4(c), the 1st and 2nd shock waves have merged in the position of PS1, and the formed precursor shock wave is in coupled state with the flame which indicates the formation of detonation. Based on these experimental results, the detonation limit is within the initial pressure range of 0.25-0.30 atm.

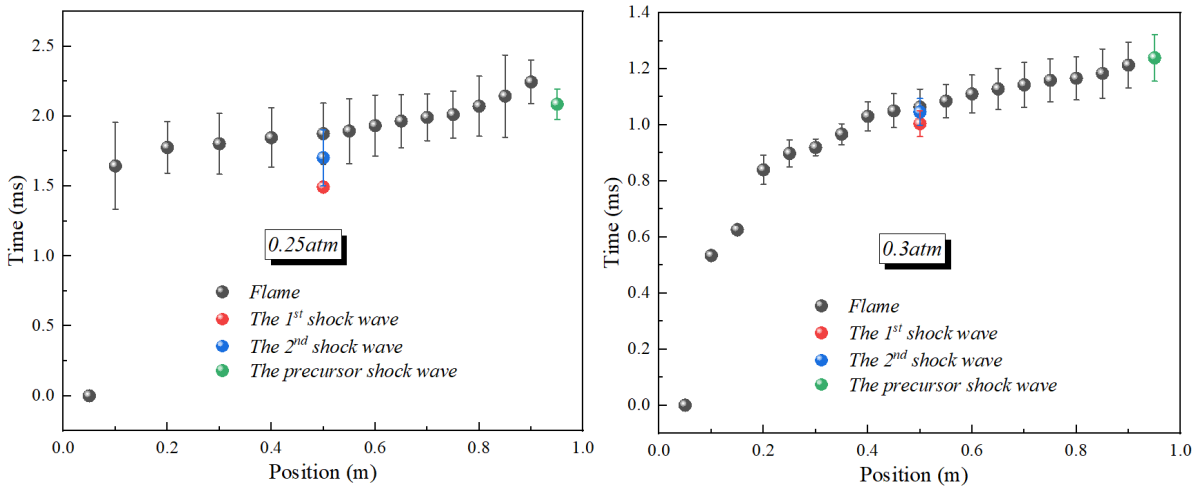

(a) (b)

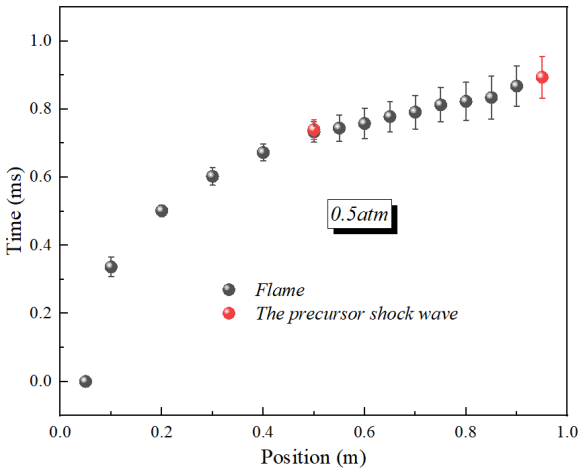

(c)

Figure 4. The positions of shock waves and flame versus corresponding time instants at different P_0 and 77 K with the equivalence ratio of 1.5.

3.2 Strong flame acceleration (FA)

The flame velocity versus position at 77 K and different P_0 with the equivalence ratio of 1.5 is showed in Fig. 5. From Fig. 5, at 0.20-0.50 atm, all flames firstly accelerate to supersonic state in a relatively shorter distance. In the flame acceleration stage, the expansion ratio describing the expansion of the hot combustion products and the maximum temperature gradient controlling the thermal diffusion from the hot combustion products to cold unburned reactants are two factors that will promote the flame to accelerate. In present study, at the same initial pressure of 0.50 atm, the decrease in initial temperature from 300 K to 77 K results in 3.5 times larger expansion ratio. And, the cryogenic temperature also increases the maximum temperature gradient compared with the room temperature. Thus, the increasing expansion ratio and the increasing maximum temperature gradient all promote the flame to accelerate fast at cryogenic temperature.

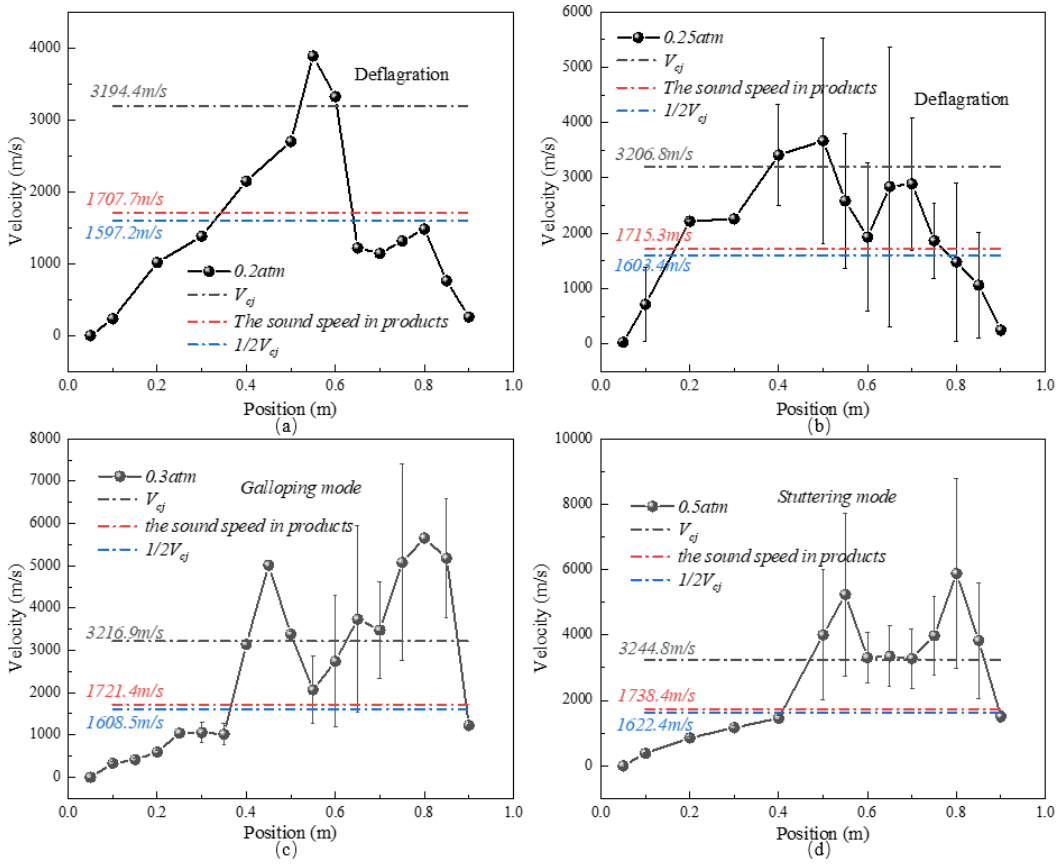

Figure 5. The flame velocity versus position at different P_0 and 77 K with equivalence ratio of 1.5.

In addition, Kuznetsov et al. [1] illustrated that, for the hydrogen-air mixtures, with the same flow velocity, the two times lower sound speed and the larger adiabatic coefficient results in 2-3 times higher dynamic pressure at 100K compared with the ambient temperature. All these factors will promote the faster FA and DDT at cryogenic temperature. In present study, with the equivalence ratio of 1.5 for hydrogen-oxygen mixture, the cryogenic temperature of around 77 K leads to the 2 times lower sound speed than 300 K. And, the 2 times lower sound speed will cause the 2 times higher Mach number at 77 K than 300 K with the same flow velocity. Together with the larger adiabatic coefficient, the dynamic pressure at 77 K is almost 4 times higher than that at 300 K.

Dorofeev et al. [10] found that there are two different acceleration regimes for different mixtures: one is the strong FA which results in the supersonic flame, and the other is the weak FA which leads to the slow velocity flame. And, they found that the expansion ratio is the main factor that induces these two different flame acceleration regimes. In order to define the critical condition between the strong FA and the weak FA, Dorofeev et al. [11] proposed a model to evaluate the flame acceleration potentiality of mixture via analyzing the re-ignition/quenching of the largest mixed pockets. And the model is shown in Eq. (1).

$$\frac{\sigma^2\beta^2(\beta/2-1)^n e^{1-\beta/2}}{6Le_{eff}^n \Gamma_{n+1}\mu} = 1, \tag{1}$$

where, Le_{eff} and n are the effective Lewis number [12] and the overall reaction order [13], respectively. $\Gamma_{n+1} \equiv \int_0^\infty \xi^n e^{-\xi} d\xi$ is the Gamma function and μ is a constant of 20.

As a result of the effect of flame instabilities (e.g. the D-L, T-D and R-T instabilities) on flame front, the initial laminar flame gradually becomes the turbulent flame. And, in the initial stage of the interaction between the turbulent flow and the flame, the increase in flame surface area and turbulence intensity will produce positive feedback for FA. However, at a certain stage, there are many mixed pockets formed in the flow ahead of flame, as a result of the mixing of the burned products and the unburned mixtures. The model of Eq. (1) can be used to estimate whether the positive feedback for FA can be maintained or not. If the left side of Eq. (1) is larger than 1, the

largest mixed reactants/products pockets has not influence on the energy release rate and the positive feedback for FA will be maintained. If the left side of Eq. (1) is lower than 1, this indicates that the positive feedback for FA will be destroyed due to the quenching effect of mixed pockets will suppress the energy release rate.

Table 1. The calculation results at different initial pressures with Eq. (1) at equivalence ratio of 1.5.

P_0 (atm)	77 K
0.20	13.546
0.25	14.552
0.30	15.559
0.50	19.865

The calculated results of left side of Eq. (1) at different initial pressures and 77 K with the equivalence ratio of 1.5 is shown in Table 1. From Table 1, the calculated results at 0.20-0.50 atm are all larger than 1 which means the re-ignition effect of mixed pockets will not influence the energy release rate and the positive feedback for FA will be maintained. Thus, the strong FA regime will be formed in these mixtures, which is consistent with the experimental results as showed in Fig. 5.

3.3 Flame regimes and detonation limit

From Fig. 5, at 0.25-0.50 atm, all flames firstly accelerate to around half of the C-J detonation velocity ($0.5V_{cj}$) or the sound speed in products before the deflagration to detonation transition occurs. At 0.20 and 0.25 atm, after accelerating rapidly to V_{cj}, flames then decay to fluctuate around $0.5V_{cj}$ due to the energy release could not maintain the propagation of detonation, and finally the re-ignition of detonation has not occurred. This mode is considered as the deflagration mode. With the increase in the initial pressure to 0.30 atm, the periodic velocity fluctuation between V_{cj} and $0.5V_{cj}$, which means the periodic re-ignition and failure of detonation, is observed. This mode is considered as the galloping mode which has been observed in many studies [14-16]. With the further increase in initial pressure to 0.50 atm, after DDT occurs, the flame velocity mainly distributes around V_{cj} and this mode is defined as the stuttering mode. In summary, the deflagration, the galloping mode and the stuttering mode are captured with the initial pressure increases from 0.20 atm to 0.5 atm in present study. Thus, the detonation limit is within 0.25-0.3 atm. In addition, based on above descriptions, there is a critical state in which flame propagates at the speed of $0.5V_{cj}$ during the onset or failure stage of detonation. The critical state is regarded as the C-J deflagration which is made up of the turbulent reaction zone and a leading shock wave and propagates forward with the speed of $0.5V_{cj}$ [17-19].

The galloping mode, an unstable near limit detonation mode, is generally observed in unstable mixture near the limit condition [16]. For the aim of defining the boundary between the unstable mixture and the stable mixture, Radulescu [17, 20] proposed a stability parameter χ_1 which controls the detonation cell structure. The detonation cell structure is irregular in unstable mixture, while in stable mixture, the detonation cell becomes regular. And, the boundary between the regular detonation cell structure and the irregular detonation cell structure is found be $\chi_1 = 10$, and when $\chi_1 > 10$, the detonation cell structure shows an irregular shape. Thus, when the stability parameter χ_1 is higher than 10, the mixture is the unstable mixture. The stability parameter is defined as Eq. (2).

$$\chi_1 = \frac{t_i}{t_e}\frac{E_a}{RT_s}, \tag{2}$$

where, t_i and t_e are the induction time and the reaction time, respectively. E_a/RT_s is the normalized activation energy behind detonation shock wave. And more details about the parameters in Eq. (2) can be found in [2, 17, 20].

The calculated results at different initial pressures and 77 K with the equivalence ratio of 1.5 are shown in Table 2. From Table 2, the stability parameters at 0.20-0.50 atm are all higher than 10 which means the mixture of hydrogen-oxygen with the equivalence ratio of 1.5 is unstable mixture. As a result of unstable mixture, in present study, the galloping mode is observed near the limit condition.

Table 2. The calculated results of χ_1 parameter at 77 K with the equivalence ratio of 1.5.

P_0 (atm)	t_i/t_e	E_a/RT_s	χ_1
0.20	9.521	7.954	75.728
0.25	8.684	7.434	64.559
0.30	8.986	8.154	73.270
0.50	9.457	9.887	93.498

3.4 Heat loss effect

The heat loss effect on flame propagation will be enhanced at the cryogenic temperature condition. The heat loss to tube wall has been investigated in many studies [21-23]. The detonation limit theory considering the heat and moment loss to tube wall shows the lower tube diameter will increase the specific surface area which increases the heat loss to tube wall and the larger detonation velocity deficits [21]. Daou and Matalon [22] found that there are two modes, including partial extinction in wider channels and total extinction in narrow channels. The balance between the heat release rate and the heat loss rate controls the detonation limit [23].

Rubtsov [24, 25] proposed a model considering the heat loss and the chemical loss to analyze the energy loss effect on the detonation limit. In present study, for the aim of analyzing the heat loss effect on detonation limit, the chemical loss in the model is assumed to be zero. Based on this model, the critical heat loss (H_{loss}) controlling the appearance of detonation limit is calculated and the detonation is possible only below the critical heat loss. And, the model is displayed as Eq. (3)-Eq. (6).

$$\frac{D^2}{2(k^2-1)} = Q - \frac{C_P R T_S^2 H_{loss} e^{Ea/RTs}}{Q E_a}, \tag{3}$$

$$k/(k-1) = C_p/R, \tag{4}$$

$$\mu = 2E_a C_p/R[1-(k-1)^2/(k+1)^2], \tag{5}$$

$$T_s = D^2[1-(k-1)^2/(k+1)^2]/C_p, \tag{6}$$

where, D is the detonation wave velocity with the specific heat loss, and when the detonation limit appears, $D^2 = V_{cj}^2 - 2V_{cj}^4/\mu$. And, V_{cj}, R, C_p, E_a and Q are the detonation wave velocity without heat loss, the universal gas constant, the heat capacities at constant pressure, the activation energy, and the chemical reaction heat release, respectively. And, H_{loss} is the heat loss when the detonation limit appears. The critical ratio of heat loss to heat release is $H_c = H_{loss}/Q$.

For the aim of analysing the heat loss effect on the detonation limit, the actual ratio of heat loss to heat release (H) needs to be estimated. For the micro-scale combustion in a cylindrical channel, the convective heat loss normalized by the chemical heat release could be calculated with the Eq. (7) [26].

$$H = \frac{Heat\ loss\ to\ the\ wall}{Total\ chemical\ heat\ release} = \frac{4{\delta_f}^2}{d^2} N_u, \tag{7}$$

$$N_u = hL/\lambda_g, \tag{8}$$

where, N_u, L and λ_g are the Nusselt number, characteristic length and the thermal conduction coefficient, respectively. And, h is the heat transfer coefficient which can be calculated with Eq. (9) [27].

$$h = 0.0055 \times \frac{\lambda_g}{l} \times {R_e}^{0.44} \times {P_r}^{0.4}, \tag{9}$$

where, R_e and P_r are the Reynolds number and the Prandtl Number, respectively.

The relationship between the theoretical critical ratio of heat loss to heat release (H_c) and the actual ratio of heat loss to heat release (H) at different P_0 and 77 K with the equivalence ratio of 1.5 is shown in Fig. 6. Only when H is lower than the critical value H_c, the heat loss effect can not cause the failure of detonation. From Fig. 6, the critical value H_c is two orders of magnitude larger than H which means the detonation is possible and the heat loss effect on the detonation is weak. The experimental results show that the stuttering the galloping detonation modes are observed at 0.50 atm and 0.30 atm, respectively. The deflagration mode is captured at 0.20 and 0.25 atm, and it is the lower heat release causing by lower initial pressure instead of the heat loss effect that causes the failure of detonation. Thus, the experimental results are consistent with the prediction results of above model.

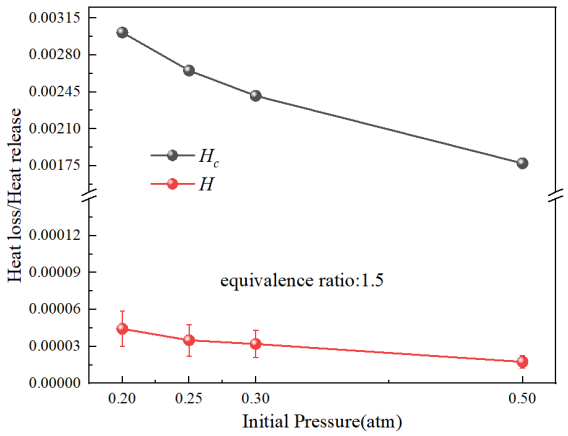

Figure 6. The ratio of heat loss to heat release as function of initial pressure at 77 K with equivalence ratio of 1.5.

3.5 Detonation cell regularity

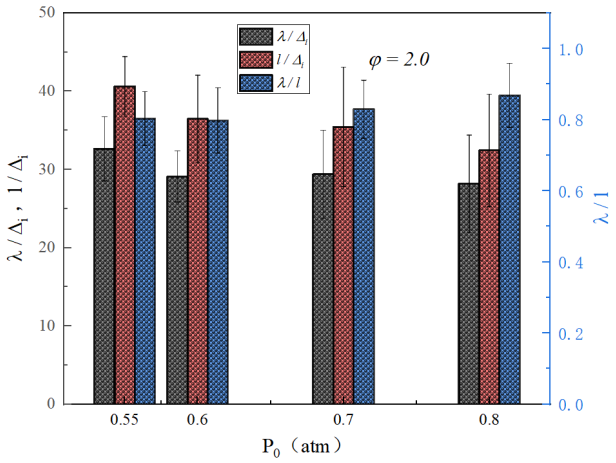

Figure 7. The statistics results of the cell width λ, the cell length l and the ratio of cell width to cell length λ/l at different initial pressures and 77 K with the equivalence ratio of 2.0.

Detonation cells are formed with the triple-shock collisions in which the interactions of transverse waves play an important role, especially for the unstable mixture. As a result of transverse wave interactions, the characteristic scales of detonation cells (e.g. the cell length l and the cell width λ) also describe the propagation behaviours of transverse waves in return. The cell length l shows the frequency of transverse waves interactions, and the density of transverse waves can be measured with the cell width λ [28]. For the aim of investigating the regularity of detonation cells, in present study, the detonation cells of hydrogen-oxygen with the equivalence ratio of 2.0 were measured. For each of experiment cases, more than 50 detonation cells are measured by reading the pixels method for the statistics of characteristic scales of detonation cells. The statistics results of the cell width normalized by the induction length λ/Δ_i, the cell length normalized by the induction length l/Δ_i and the ratio of cell width to cell length λ/l at different initial pressures and 77 K with the equivalence

ratio of 2.0 are showed in Fig. 7. From Fig. 7, the ratio of cell width to cell length basically maintains constant at different initial pressures.

Generally, there is a certain link between the detonation cell width and the induction length (Δ_i), such as $\lambda = A\Delta_i$, and A is a specific coefficient. For the aim of predicting the detonation cell size, Ng et al. [29] proposed a model to describe the variation of the coefficient A via considering the detonation instability effect, and the accuracy of this model has been verified by many studies [29-31]. The model is showed with Eq. (10).

$$\lambda = A(\chi_2) \cdot \Delta_i = [A_0 + (a_N/{\chi_2}^N + \cdots a_1/\chi_2 + b_1\chi_2 + \cdots b_N{\chi_2}^N)] \cdot \Delta_i, \quad (10)$$

where, Δ_i is the induction length, and the other coefficients a_k and b_k are shown in Table 3.

Table 3. The coefficients a_k and b_k in model of Eq. (11) proposed by Ng et al. with $N = 3$ [29].

Coefficients	Values
A_0	30.466
a_1	89.554
a_2	-130.793
a_3	42.025
b_1	-0.02929
b_2	1.0263e-05
b_3	-1.0319e-09

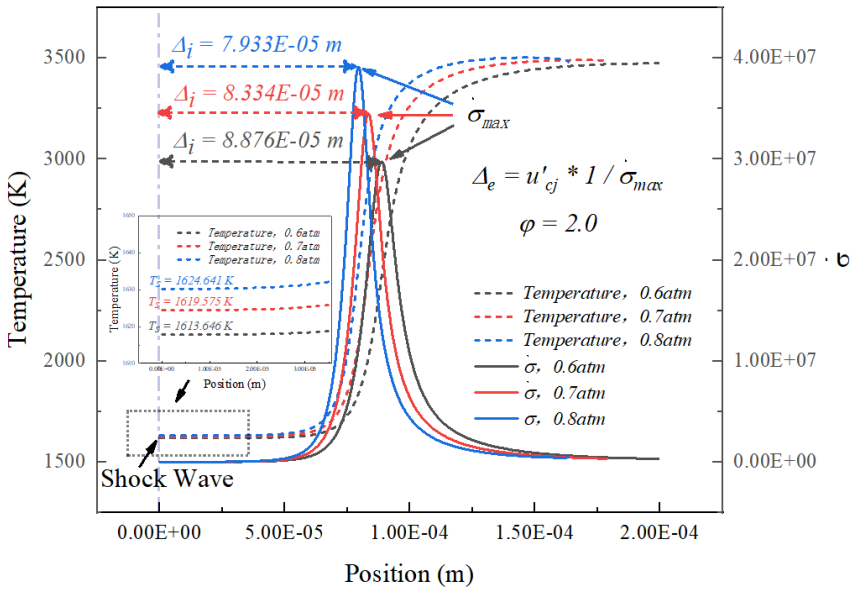

Figure 8. The one-dimensional ZND detonation profiles at 0.6-0.8 atm with the equivalence ratio of 2.0.

In this model, the stability parameter χ_2 is defined as Eq. (11).

$$\chi_2 = \frac{\Delta_i}{\Delta_e}\frac{E_a}{RT_s} = \Delta_i \frac{\dot{\sigma}_{max}}{u'_{cj}}\frac{E_a}{RT_s}, \quad (11)$$

where, Δ_e is the reaction zone length which is defined by the inverse of the maximum thermicity ($1/\dot{\sigma}_{max}$) multiplied by the particle velocity u'_{cj}. And, the one-dimensional ZND detonation profiles at 0.6-0.8 atm with the equivalence ratio of 2.0 is showed in Fig. 8. From Fig. 8, the induction length is defined as the distance between the shock wave and the maximum thermicity, and the increase in initial pressure could result in the increase in the post-shock temperature (T_s) which causes the shorter induction length and the lower maximum thermicity $\dot{\sigma}_{max}$.

And, the experimental and predicted results of detonation cell width at different initial pressures and 77 K with the equivalence ratio of 2.0 are showed in Fig. 9. From Fig. 9, the prediction results of detonation cell width are basically consistent with the experimental results. With the increase in initial pressure, the detonation cell width decreases which means the stronger detonation ability at larger initial pressure.

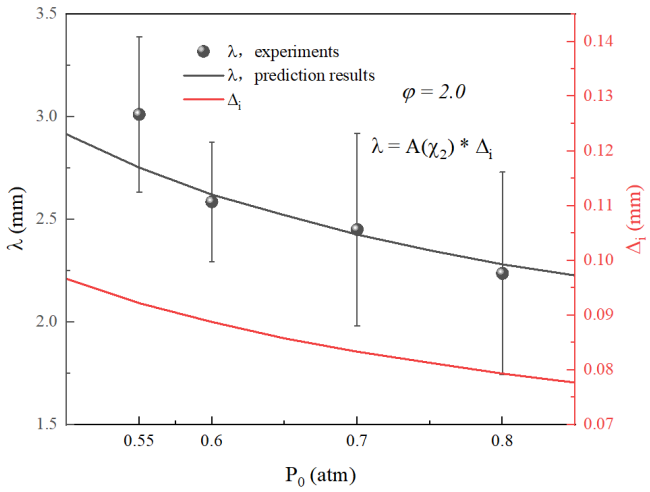

Figure 9. The experimental and predicted results of detonation cell width at different initial pressures and 77 K with the equivalence ratio of 2.0

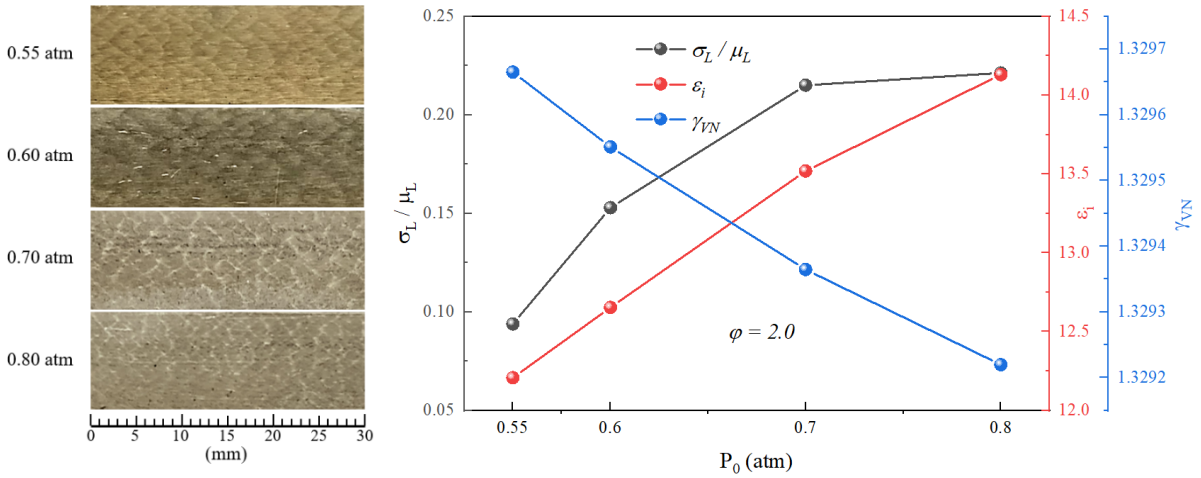

(a) (b)

Figure 10. The measured smoked foils (a) and the parameter σ_L/μ_L (b) at different initial pressures and 77 K with the equivalence ratio of 2.0.

For the aim of analysing the regularity of detonation cell structure, Meagher et al. [28] found the post-shock specific heat ratio γ_{VN} and the normalized activation energy ε_i, which represents the gasdynamic effect and the chemistry effect, respectively, play an important role in the detonation cell regularity. They proposed a parameter σ_L/μ_L to evaluate the regularity of detonation cells, and the parameters σ_L and μ_L are the standard deviation and the mean value of the normalized cell length l/Δ_i, respectively. The measured smoked foils (a) and the parameter σ_L/μ_L (b) at different initial pressures and 77 K with the equivalence ratio of 2.0 are showed in Fig. 10.

From Fig. 10(a), the increase in initial pressure will results in the more irregular detonation cell, which can be well predicted with the parameter σ_L/μ_L in Fig. 10(b). When the parameter σ_L/μ_L is lower, this means the more regular detonation cell. The decrease in γ_{VN} will lead to the occurrence of the Mach stem bifurcations which causes the irregular detonation cell structure [28]. And, the

increasing ε_i will cause the greater variation of the transverse wave strength and transition from cell-driven to transverse-detonation-driven burning which results in the more irregular detonation cell [28]. From Fig. 10(b), the lower initial pressure causes the larger γ_{VN} and the lower ε_i which all lead to the regular detonation cell structure.

4.0 CONCLUSIONS

In present study, the strong flame acceleration, detonation limit, the heat loss effect on detonation limit and the regularity of detonation cell are analysed and the main conclusions are as follows:

(1) The 1st and 2nd shock waves are captured and they finally merge to form a stronger precursor shock wave prior to the onset of detonation.

(2) The strong flame accelerations caused by sufficiently larger expansion ratio are observed at considered cases.

(3) The stuttering mode, the galloping mode and the deflagration mode are observed when the initial pressure decreases from 0.50 atm to 0.20 atm with the equivalence ratio of 1.5. And, the detonation limit is within the initial pressure range of 0.25 atm to 0.30 atm.

(4) The heat loss effect on detonation limit is analysed.

(5) The decreases in initial pressure will cause the larger γ_{VN} and the lower ε_i which all lead to the regular detonation cell structure.

REFERENCES

1. Kuznetsov, M., Denkevits, A., Veser, A., Friedrich, A., Necker, G. and Jordan, T., Shock tube experiments on flame propagation regimes and critical conditions for flame acceleration and detonation transition for hydrogen-air mixtures at cryogenic temperatures, Int. Conf. on Hydrogen Safety, 2021.
2. Shen, X., Fu, W., Liang, W., Wen, J.X., Liu, H. and Law, C.K., Strong flame acceleration and detonation limit of hydrogen-oxygen mixture at cryogenic temperature, Proceedings of the Combustion Institute, 2022.
3. Manson, N. and Guénoche, H., Effect of the charge diameter on the velocity of detonation waves in gas mixtures, Symposium (International) on Combustion, Elsevier, 1957.
4. Kogarko, S. and Zel'dovich, Y.B., On detonation of gas mixtures, Dokl. Akad. Nauk SSSR, 1948.
5. Kuznetsov, M., Alekseev, V., Matsukov, I. and Dorofeev, S.B., DDT in a smooth tube filled with a hydrogen–oxygen mixture, Shock waves, 14, No. 3, 2005, pp. 205-215.
6. Kuznetsov, M., Matsukov, I., Alekseev, V., Breitung, W. and Dorofeev, S.B., Effect of boundary layer on flame acceleration and DDT, Proc. 20th, 2005.
7. Kellenberger, M. and Ciccarelli, G., Advancements on the propagation mechanism of a detonation wave in an obstructed channel, Combustion and Flame, 191, 2018, pp. 195-209.
8. Cheng, J., Zhang, B., Liu, H. and Wang, F., Experimental study on the effects of different fluidic jets on the acceleration of deflagration prior its transition to detonation, Aerospace Science and Technology, 106, 2020.
9. Cheng, J., Zhang, B., Liu, H. and Wang, F., The precursor shock wave and flame propagation enhancement by CO_2 injection in a methane-oxygen mixture, Fuel, 283, 2021.
10. Dorofeev, S.B., Kuznetsov, M., Alekseev, V., Efimenko, A.A. and Breitung, W., Evaluation of limits for effective flame acceleration in hydrogen mixtures, Journal of Loss Prevention in the Process Industries, 14, No. 6, 2001, pp. 583-589.
11. Dorofeev, S.B., Thermal quenching and re-ignition of mixed pockets of reactants and products in gas explosions, Proceedings of the Combustion Institute, 31, No. 2, 2007, pp. 2371-2379.
12. Bouvet, N., Halter, F., Chauveau, C. and Yoon, Y., On the effective Lewis number formulations for lean hydrogen/hydrocarbon/air mixtures, International Journal of Hydrogen Energy, 38, No. 14, 2013, pp. 5949-5960.

13. Egolfopoulos, F.N. and Law, C.K., Chain mechanisms in the overall reaction orders in laminar flame propagation, Combustion and Flame, 80, No. 1, 1990, pp. 7-16.
14. Lee, J.J, Dupré, G., Knystautas, R. and Lee, J.H., Doppler interferometry study of unstable detonations, Shock Waves, 5, No. 3, 1995, pp. 175-181.
15. Gao, Y., Ng, H.D. and Lee, J.H., Experimental characterization of galloping detonations in unstable mixtures, Combustion and Flame, 162, No. 6, 2015, pp. 2405-2413.
16. Haloua, F., Brouillette, M., Lienhart, V. and Dupré, G., Characteristics of unstable detonations near extinction limits, Combustion and flame, 122, No. 4, 2000, pp. 422-438.
17. Radulescu, M.I., The propagation and failure mechanism of gaseous detonations: experiments in porous-walled tubes, Ph.D. Thesis, McGill University, 2003.
18. Zhu, Y.J., Chao, J. and Lee, J.H., An experimental investigation of the propagation mechanism of critical deflagration waves that lead to the onset of detonation, Proceedings of the Combustion Institute, 31, No. 2, 2007, pp. 2455-2462.
19. Chue, R.S., Clarke, J.F. and Lee, J.H., Chapman-Jouguet deflagrations, Proc. R. Soc. Lond. A, 441, No. 1913, 1993, pp. 607-623.
20. Tang, J. and Radulescu, M.I., Dynamics of shock induced ignition in Fickett's model: Influence of χ, Proceedings of the Combustion Institute, 34, No. 2, 2013, pp. 2035-2041.
21. Zel'dovich, Y.B., On the theory of the propagation of detonation in gaseous systems, Zh. eksp. teoret. fiz., 10, 1940, pp. 542-568.
22. Daou, J. and Matalon, M., Influence of conductive heat-losses on the propagation of premixed flames in channels, Combustion and Flame, 128, No. 4, 2002, pp. 321-339.
23. Kitano, S., Fukao, M., Susa, A., Tsuboi, N., Hayashi, A. and Koshi, M., Spinning detonation and velocity deficit in small diameter tubes, Proceedings of the combustion institute, 32, No. 2, 2009, pp. 2355-2362.
24. Rubtsov, N.M., Effect of chemically active additives on the velocity of detonation waves and on the limit of gaseous detonation, Mendeleev Communications, 10, No. 6, 2000, pp. 225-227.
25. Rubtsov, N.M., Effect of chemically active additives on the detonation wave velocity and detonation limit in rich mixtures, Theoretical Foundations of Chemical Engineering, 39, No. 3, 2005, pp. 275-282.
26. Lei, Y., Chen, W. and Lei, J., Combustion and direct energy conversion inside a micro-combustor, Applied Thermal Engineering, 100, 2016, pp. 348-355.
27. Nitsche, M. and Gbadamosi, R.O., Design of Evaporators, Heat Exchanger Design Guide, 2016, pp. 147-179.
28. Meagher, P.A., Shi, X., Santos, J.P., Muraleedharan, N.K., Crane, J., Poludnenko, A.Y., Wang, H. and Zhao, X., Isolating gasdynamic and chemical effects on the detonation cellular structure: A combined experimental and computational study, Proceedings of the Combustion Institute, 2022.
29. Ng, H.D., Chao, J., Yatsufusa, T. and Lee, J.H., Measurement and chemical kinetic prediction of detonation sensitivity and cellular structure characteristics in dimethyl ether–oxygen mixtures, Fuel, 88, No. 1, 2009, pp. 124-131.
30. Zhang, B., Pang, L., Shen, X. and Gao, Y., Measurement and prediction of detonation cell size in binary fuel blends of methane/hydrogen mixtures, Fuel, 172, 2016, pp. 196-199.
31. Hou, Y., Liu, X., Lv, X., Yu, X., Yan, X. and Yu, J., Detonation behaviors of stoichiometric H2-O_2 mixture diluted with He, N_2, CO_2 at different initial pressures, Fuel, 330, 2022.